Local Fe structure and ferromagnetism in Fe-doped ZnO films

2006 J. Phys.: Condens. Matter 18 7471

(http://iopscience.iop.org/0953-8984/18/31/037)

INSTITUTE OF PHYSICS PUBLISHING JOURNAL OF PHYSICS: CONDENSED MATTER

J. Phys.: Condens. Matter **18** (2006) 7471–7479 doi:10.1088/0953-8984/18/31/037

Local Fe structure and ferromagnetism in Fe-doped ZnO films

X X Wei[1], C Song[1], K W Geng[1], F Zeng[1], B He[2] and F Pan[1,3]

[1] Laboratory of Advanced Materials, Department of Materials Science and Engineering, Tsinghua University, Beijing 100084, People's Republic of China
[2] National Synchrotron Radiation Laboratory, University of Science and Technology of China, Hefei, 230029, People's Republic of China

E-mail: panf@mail.tsinghua.edu.cn

Received 21 June 2006, in final form 30 June 2006
Published 21 July 2006
Online at stacks.iop.org/JPhysCM/18/7471

Abstract

The local Fe structure and corresponding ferromagnetism are different for various concentrations of Fe-doped ZnO ($Zn_{1-x}Fe_xO$, $x = 0$–0.07) films, which are prepared on $LiNbO_3$(104) substrates by reactive magnetron sputtering. X-ray photoelectron spectroscopy and x-ray absorption near-edge structure (XANES) reveal that, when $x \leqslant 0.04$, Fe is in the 2+ state and is incorporated into the wurtzite lattice of ZnO, and as x increases further, a second phase Fe_3O_4 is induced. Furthermore, full multiple-scattering substitution *ab initio* calculation of Fe K-edge XANES is used to confirm the local structure of Fe in films with different x. The single-phase Fe-doped ZnO films ($x \leqslant 0.04$) exhibit ferromagnetism above room temperature and the mechanism of bound magnetic polarons (BMPs) is proposed to discuss the magnetic properties. The presence of the second phase is responsible for the strong ferromagnetism for higher Fe concentration.

1. Introduction

Diluted magnetic semiconductors (DMSs) have attracted broad interests recently for their use as the materials of spintronics [1]. Both theoretical and experimental realization of ferromagnetic semiconductors could lead to new classes of devices. There is already a technology based on proposing candidate materials (such as GaN, GaP and ZnO) and a fairly good understanding of the basic electrical and optical properties. The introduction of transitional metals into these materials under the right conditions is found to produce ferromagnetism near or above room temperature [2]. The mechanism for the ferromagnetism is still in debate since the models that are used to explain the ferromagnetism such as the carrier-induced, double-exchange and bound magnetic polaron all potentially play a role depending on the conductivity type and level in the materials [3].

[3] Author to whom any correspondence should be addressed.

Specifically, ZnO, which has a large band gap (3.37 eV) and exciton binding energy (60 meV), excellent mechanical characteristics, and is inexpensive and environmentally safe, has been identified as a promising host material [4]. From reviewing recent experimental work, we can find that most studies were done with Co-doped ZnO, which shows interesting properties [5, 6]. Since the structures of Co and ZnO are isomorphous and the atomic size of Co^{2+} and Zn^{2+} is similar, Co-doped ZnO always shows a high thermal solubility and ferromagnetism above room temperature. In contrast, ZnO doped with Fe has been confirmed experimentally to exhibit ferromagnetism (FM) at room temperature [7], though in many cases the Fe-doped ZnO does not have a large magnetic moment [8–10]. Due to the low solution limit of Fe in ZnO [11], second phases form when the Fe ions are not fully diluted into the matrix, such as Fe clusters or some iron oxides [10, 12]. Besides the need for materials with a high Curie temperature (T_c) along with high magnetic moments, it is more important to assure that the dopant atoms are well dissolved into the oxide host to be really diluted and that the resulting FM indeed originates from the doped matrices [13]. So far, several inconsistent results have been attained: Venkatesan *et al* found high temperature ferromagnetic ordering with a saturation magnetic moment of 0.8 μ_B/Fe for Fe-doped ZnO, whereas paramagnetic behaviour was reported by other groups [6]. Though the origin of the ferromagnetism in these systems is uncertain, incomplete sample characterization to rule out secondary phases is a common cause of controversy.

Doped ZnO films have been deposited by different kinds of methods on various substrates. For Co:TiO_2 films the dependence of magnetic behaviour on the use of various substrates has been discussed specifically [5, 6], which shows using a ferroelectric such as $SrTiO_3$ and $LaAlO_3$ as the substrate will lead to a stronger ferromagnetism than using Si or Al_2O_3 substrate. Though few direct substrate-dependent magnetization studies have been published for doped ZnO films, previous results reveal that the magnetic behaviour varies when using different substrates [6]. For Co-doped ZnO films, we have found a giant magnetic moment of 6.1 μ_B/Co when the film is deposited on $LiNbO_3$ [14], which is higher than that of most films deposited on other substrates with counterpart Co concentration.

In this work, we also deposit ZnO films on the ferroelectric substrate $LiNbO_3$(104) by reactive magnetron Fe-spurting. The control samples deposited on different kinds of other substrates as well as the influence of the substrate on the magnetization will be discussed in detail in a subsequent paper. X-ray absorption near-edge structure (XANES) as well as a full multiple-scattering substitution *ab initio* calculation is used to elucidate the geometry of Fe in ZnO films and the bound magnetic polarons (BMPs) model is adopted to explain the magnetic properties.

2. Experiment

Various concentrations of Fe-doped ZnO ($Zn_{1-x}Fe_xO$, $x = 0$–0.07) films were deposited on the (104) plane of $LiNbO_3$ (LN) single-crystal substrates by direct current reactive magnetron Fe-sputtering. The relative sputtering area of Fe chips which were attached on a Zn target (99.999% purity) determines the Fe composition in the deposited Fe-doped ZnO films. The base pressure of the sputter deposition chamber was 3×10^{-6} Torr and the working pressure was a mix of argon and oxygen at 2.5×10^{-3} Torr and 4.1×10^{-3} Torr respectively. The deposition rate was 0.05 nm s^{-1} and the substrate temperature during the process of depositing was ∼200 °C. Thermal annealing was performed at 750 °C in air for 1 h.

The crystal structure and crystalline quality of the ZnO films were investigated by θ–2θ x-ray diffraction (XRD) using Cu Kα (0.154 06 nm) radiation. The angular spread of the (002) plane around the maximum (002) peak position was determined by x-ray rocking curve

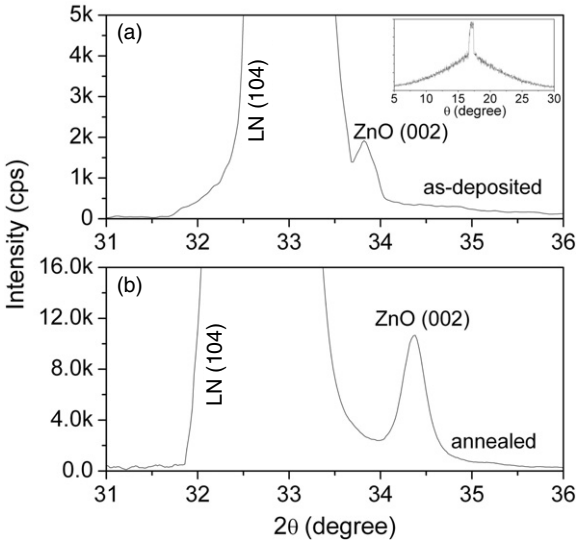

Figure 1. XRD patterns of the $Zn_{0.96}Fe_{0.04}O$ film as-deposited (a) and annealed in air at 750 °C for 1 h (b).

measurements. The thickness and surface morphology were characterized by surface electron microscopy (SEM). High-resolution transmission electron microcopy (HRTEM) imaging and selected area electron diffraction (SAED) were used to study the interface boding and structural characteristics. X-ray photoelectron spectroscopy (XPS) spectra were characterized to verify the Fe composition of films and the valence state of Fe in the ZnO films. X-ray-absorption near-edge spectrum (XANES) at the Fe K-edge was measured to confirm the valence sate and local geometry of the Fe dopant in the ZnO lattice. The magnetic properties of the film were studied by a vibrating sample magnetometer (VSM) with the magnetic field parallel to the films. High-temperature magnetization (300 K $\leqslant T \leqslant$ 800 K) was recorded using a VSM. Induced-coupled-plasma (ICP) atomic emission spectra were used to determine the Fe contents in the samples in order to calculate the average magnetic moment per Fe atom.

Furthermore, the Fe K-edge XANES spectrum was simulated via the full multiple-scattering (MS) theory using the *ab initio* self-consistent free energy force field (FFFF) 8.2 code with two complementary modes: MS scattering and path analysis of only the most important scattering paths [15]. Within the FFFF code, exchange parameters were justified to correct for any offset in the calculated Fermi energy level, generally a negative shift of 3 eV. For the exchange correlation part of the potential, in order to simulate the atomic bond, the energy and position dependent optical Hedin–Lundqvist potential with a muffin-tin radii overlap of 10% between contiguous spheres were used. These conditions have been found to produce good potentials for an accurate XANES calculation of complex transition metal oxides [15, 16].

3. Results and discussion

For $Zn_{1-x}Fe_xO$ films, when $x \leqslant 0.04$, the XRD analysis shows that these samples remain a single phase. Figure 1 shows the XRD patterns of $Zn_{0.96}Fe_{0.04}O$ as-deposited and annealed in air grown on LN (104) substrates. It is obvious that both of them show a preferential (002) orientation. Comparing with the pure ZnO films [17] we find there is a relative shift of the (002) peak to a lower angle for Fe:ZnO, which indicates that Fe is incorporated into the wurtzite

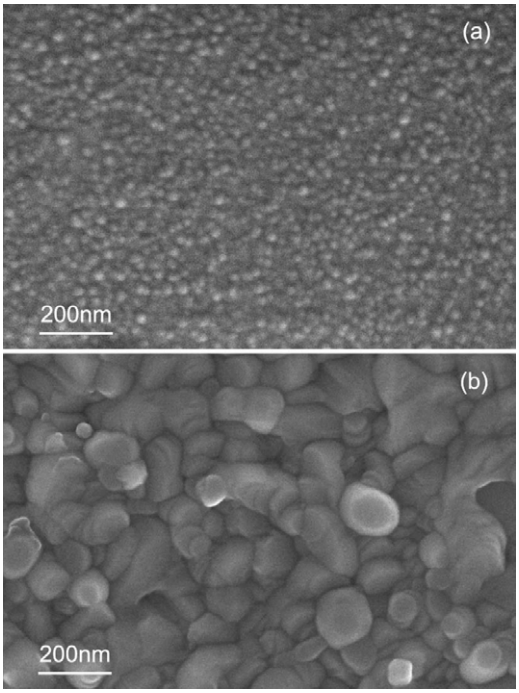

Figure 2. SEM images of the as-deposited (a) and annealed (b) Fe-doped ZnO films.

lattice [14]. After annealing, the ZnO(002) peak becomes stronger and shifts back to 34.4°, which is in good agreement with bulk ZnO, indicating that annealing relived most of the strain in the film [18]. Figure 2 shows the SEM images of the as-grown and annealed Fe-doped ZnO films. The grain sizes of the annealed sample are obviously larger than those of the as-deposited sample, which should be caused by strain relaxation. The annealing process clearly produces a recovery of the crystal structure and increase of the grain size.

Typical cross-sectional HRTEM images are shown in figure 3. Figure 3(a) shows that grains of different crystal orientations exist near the interface of the film and substrate. The lattice mismatch of ZnO ($a = 3.245$ Å, $c = 5.207$ Å, hexagonal) to the LN substrate ($a = 5.149$ Å, $c = 13.862$ Å), results in polycrystalline Fe:ZnO films instead of perfect epitaxial growth. It is well-known that it is easy for ZnO to grow as c-oriented, since the (002) crystallographic plane has the lowest surface free energy, which will lead to ZnO(001) growing parallel to the substrate. This is shown in figure 3(b), representing the ZnO film further away from the substrate (near the surface of the film). That is, the film shows strong c-oriented growth, although it is polycrystalline near the substrate. This conclusion can also be reached with the unique rocking curve shown in the inset of figure 1(a). When 2θ is fixed at 33.8° determined by the position of ZnO(002) in figure 1, and θ scans from 5° to 30°, although it is observed that the film shows an apparently c-oriented structure, the intensity on both sides of the (002) peak cannot be ignored. This indicates that the grains of (001) growth predominate while the grains of other growth also exist.

In our samples of $Zn_{1-x}Fe_xO$ ($x \leqslant 0.04$), the films obtained are single phase with a wurtzite structure. From previous results we cannot find a definite solubility limit for the dopant in ZnO, which may be due to the different growth conditions [5]. In our work, as x increases to 0.07, we find that a second phase begins to appear in the XRD pattern, shown in figure 4.

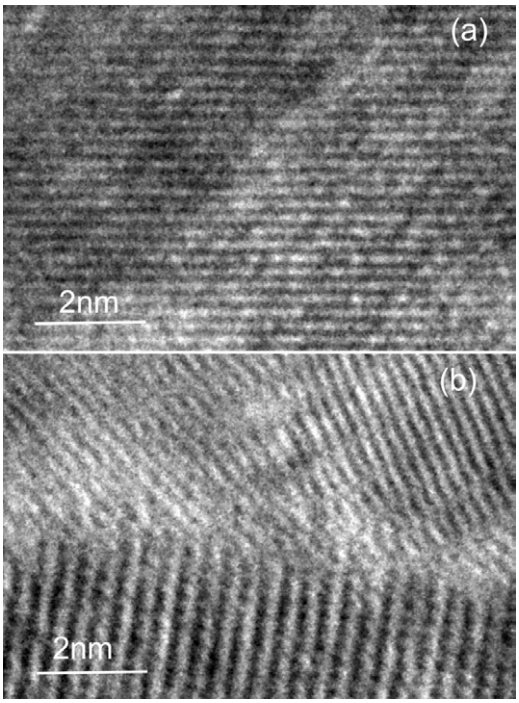

Figure 3. Typical cross-sectional HRTEM images of the area near the interface of the film and substrate (a) and the film near the surface of the film (b).

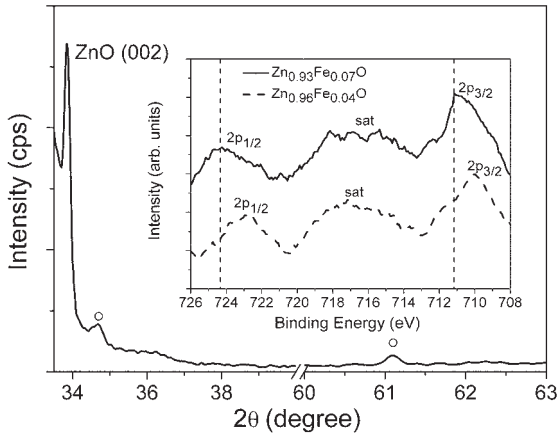

Figure 4. XRD pattern of the $Zn_{0.93}Fe_{0.07}O$ film. The inset shows the XPS spectra of $Zn_{0.96}Fe_{0.04}O$ and $Zn_{0.93}Fe_{0.07}O$ represented by a dashed line and a solid line respectively.

Some weak peaks (•) appear, which are likely assignable to Fe_3O_4. Further, from the XPS spectrum, we observe that both the Fe $2p_{1/2}$ and Fe $2p_{2/3}$ peaks of $Zn_{0.93}Fe_{0.07}O$ are between those of Fe^{3+} and Fe^{2+} in [19], and closer to Fe^{3+}, which indicates that there is a mix of 2+ and 3+ valence states, and Fe^{3+} is in the majority. In contrast, when the doped concentration $x \leqslant 0.04$, i.e., for $Zn_{0.96}Fe_{0.04}O$ shown in the inset of figure 4, the positions of the Fe $2p_{1/2}$ and

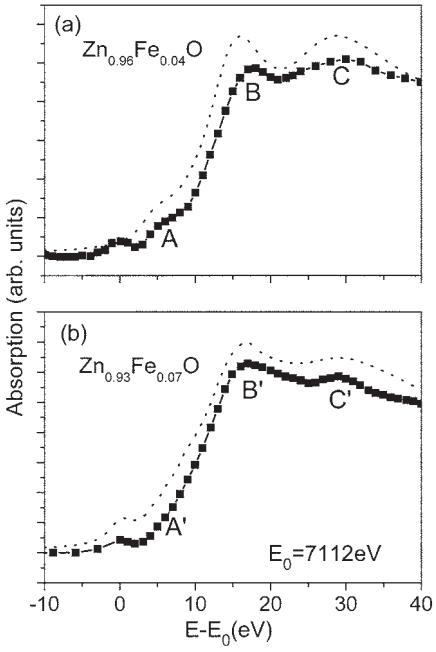

Figure 5. Fe-edge XANES spectra of $Zn_{0.96}Fe_{0.04}O$ (a) and $Zn_{0.93}Fe_{0.07}O$ (b) represented by solid lines. The corresponding MS calculations of the Fe K-edge XANES spectra are represented by lines with symbols.

Fe $2p_{2/3}$ peaks are apparently different from those of $Zn_{0.93}Fe_{0.07}O$, which reveals that Fe is in the 2+ valence state.

Although we observe the changes in XRD and XPS for different doping concentrations, it is still difficult to confirm the local structure of Fe in the films. In order to further confirm our preliminary conclusion, we employed an Fe K-edge XANES spectrum to determine the local structure of Fe in the films. The lines with symbols represent the experimental results of XANES for $Zn_{0.96}Fe_{0.04}O$ and $Zn_{0.93}Fe_{0.07}O$, shown in figures 5(a) and (b) respectively. There are two main differences between them. First, the curve for $Zn_{0.96}Fe_{0.04}O$ has an inflection at about $E - E_0 = 5$ eV ($E_0 = 7112$ eV) while the curve for $Zn_{0.93}Fe_{0.07}O$ at that position is flat (denoted with A and A′). Second, both of them have two main peaks, which are denoted with B, C and B′, C′ respectively. For $Zn_{0.96}Fe_{0.04}O$ peak C is slightly higher than peak B. However, peak B′ is apparently lower than peak C′ for $Zn_{0.93}Fe_{0.07}O$. Comparing with previous results, we find the curve for $Zn_{0.93}Fe_{0.07}O$ has some features of Fe_3O_4 [20]. Furthermore, to provide sufficient evidence, we made a full multiple-scattering *ab initio* calculation of Fe XANES at the K edge. The calculations are produced by a cluster within a sphere of radius 6 Å, which contains 77 atoms around the central Fe atom that replaces the central Zn in the ZnO atomic arrangement and 89 atoms around the Fe atom that occupies the tetrahedral site in the cubic structure of Fe_3O_4, represented by the dotted lines in figures 5(a) and (b) respectively. The most interesting result here is that the calculated spectra display similar features to the experimental spectra. Consequently, we conclude that when $x \leqslant 0.04$, Fe is in the 2+ valence state and substitutes Zn in the wurtzite lattice of ZnO, whereas as x increases beyond 0.04, Fe mainly exists in the form of Fe_3O_4.

Figure 6 reveals three typical magnetic hysteresis loops (M versus H) at 300 K of $Zn_{1-x}Fe_xO$ ($x = 0.01$, 0.04 and 0.07) films, in which the average magnetic moment is obtained

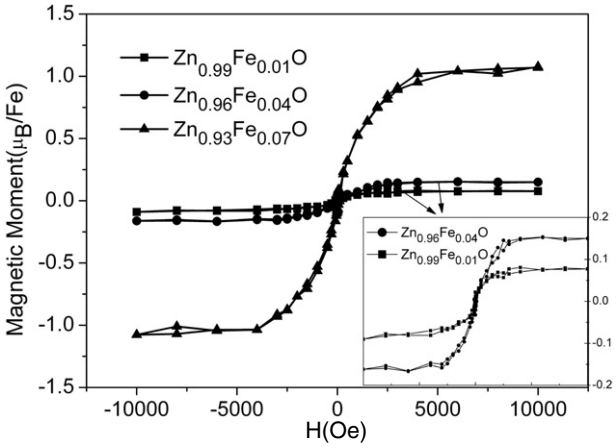

Figure 6. Typical magnetic hysteresis loops (M versus H) at 300 K of $Zn_{1-x}Fe_xO$ ($x = 0.01, 0.04$ and 0.07). The inset is the enlarged loops for $Zn_{0.99}Fe_{0.01}O$ and $Zn_{0.96}Fe_{0.04}O$.

in terms of ferromagnetism measurements. The magnetic properties of the substrate LN and the sample holder are measured first with diamagnetic magnetization; these values are subtracted automatically by computer during the measurement of Fe-doped ZnO films. From the inset (enlarged loops for $Zn_{0.99}Fe_{0.01}O$ and $Zn_{0.96}Fe_{0.04}O$), it can be clearly seen that for the samples in which Fe is incorporated into ZnO ($x \leqslant 0.04$), the films show apparent ferromagnetic properties, though the magnetization is not very high, i.e., 0.08 and 0.15 μ_B/Fe for $x = 0.01$ and 0.04. Most previous results reported by other groups reveal that it is difficult to get a very high saturation magnetization for Fe-doped ZnO [8]. It is noted that when the concentration of Fe increases to 7%, the magnetization becomes much higher ($\sim$1 μ_B/Fe), which should be mainly contributed by Fe_3O_4. For ferromagnetically coupled Fe ions in Fe_3O_4, one would expect the magnetization 1.33 μ_B/Fe [21]. This suggests that most Fe in the $Zn_{0.93}Fe_{0.07}O$ sample exists as Fe_3O_4 impurity.

Now that we have established ferromagnetism in $Zn_{1-x}Fe_xO$ at room temperature, since how to increase T_c above room temperature is a key technology in spintronics, the Curie temperature of the Fe-doped ZnO film is of interest. The inset of figure 7 shows the ferromagnetic behaviour of the single phase $Zn_{0.96}Fe_{0.04}O$ in the temperature range 300–800 K at 5000 Oe, measured by a vibrating sample magnetometer (VSM). The magnetic contribution of the substrate and holder has been subtracted from the background. It is observed that the measured magnetization shows that a transition to a paramagnetic state occurs at about 400 K, which is a high enough temperature for the purpose of device applications at room temperature. The hysteresis loops measured at 300 K after T_c measurement is also shown in figure 7, which means the Fe-doped ZnO films are annealed at a pressure of 4×10^{-6} Torr at 800 K. We observe that for $Zn_{0.96}Fe_{0.04}O$ the magnetization decreases to 0.025 μ_B/Fe, which indicates that the high-temperature process leads to a decrease of ferromagnetism. This result consists with the observed weak ferromagnetism in high-temperature processed samples in other studies [14, 22].

The wide band-gap characteristic of ZnO and the high oxygen partial pressure (4.1×10^{-3} Torr) in the reactive magnetron co-sputtering always led to a high resistivity for our ZnO films [14, 23]. In this situation the carrier density is very low, and it is inappropriate to explain the ferromagnetism with the 'carrier-mediated exchange' mechanism. Substitutionarily, a probable explanation for our samples that the Fe substituting for Zn is in the 2+ state can

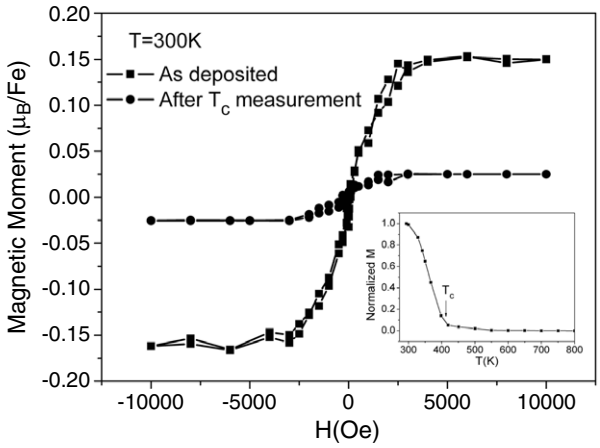

Figure 7. The hysteresis loops of $Zn_{0.96}Fe_{0.04}O$ as-deposited and measured at 300 K after T_c measurement. The inset is the normalized $(M/M_{300\,K})M$–T curve.

be found on the basis of the bound magnetic polarons (BMPs) model [6, 24]. The highly non-equilibrium process of co-sputtering makes it possible that defects in the doped films are located throughout the lattice at arbitrary distances with respect to Fe sites, which should play an important role in the system since defects in insulators with wide band gaps may offer a path to realizing unique ferromagnetic materials [25]. If neighbouring polarons do not interact strongly, a paramagnetic phase forms. However, for certain polaron–polaron distances and combinations of electron–electron and electron–local-moment exchange constants, the polarons may couple in a ferromagnetic fashion. In our low-doped samples, i.e., (1 at.%) Fe:ZnO, the polarons are too remote to perform strong exchange interaction. In contrast, there should be a proper distance between neighbouring polarons in the $Zn_{0.96}Fe_{0.04}O$ sample so that the exchange between two BMPs can become ferromagnetic. For more strongly doped films, it is possible for the magnetic moment to decrease rapidly due to the enhanced dopant–dopant associations that lead to progressive orbital moment quenching [26, 27]. But we do not observe that the ferromagnetism becomes weak, which may due to the low solubility of Fe in ZnO films. On further increasing the dopant concentration, the second phase Fe_3O_4 forms, which exhibits strong ferromagnetism. However, the drop in the magnetic moment after the T_c measurement for $Zn_{0.96}Fe_{0.04}O$ may be caused by the associations in the film.

4. Conclusion

In summary, we have studied various concentrations of Fe-doped polycrystalline ZnO ($Zn_{1-x}Fe_xO$, $x = 0$–0.07) films on $LiNbO_3$. When $x \leqslant 0.04$, Fe substitutes the Zn site in the 2+ charge state while on further increasing x to 0.07, a second phase appears and most Fe exists as Fe_3O_4. For these two cases, the specific local Fe structure is confirmed by full multiple-scattering *ab initio* calculations of the Fe K-edge XANES spectrum combined with corresponding experimental results. Compared with all other single-phase samples, $Zn_{0.96}Fe_{0.04}O$ exhibits strong ferromagnetism above room temperature ($T_c \sim 400$ K). Thus, the combination of film growth by a certain amount of iron doping and low growth temperature deposition is proved to be a significant factor in enhancing the ferromagnetism of Fe-doped ZnO. Besides, the presence of second phase Fe_3O_4 serves as an origin of higher magnetic moment for higher Fe concentration.

Acknowledgments

The authors are grateful for the financial support from the National Natural Science Foundation of China (Grant Nos. 50325105 and 50371040). Assistance from the TEM Lab and the Analysis Center of Tsinghua University is also acknowledged.

References

[1] Wolf S A, Awschalom D D, Buhrman R A, Daughton J M, von Molnár S, Roukes M L, Chthelkanova A Y and Treger D M 2001 *Science* **294** 1488
[2] Pearton S J *et al* 2003 *J. Appl. Phys.* **93** 1
[3] Pearton S J, Heo W H, Ivill M, Norton D P and Steiner T 2004 *Semicond. Sci. Technol.* **19** R54
[4] Radovanovic P V and Gamelin D R 2003 *Phys. Rev. Lett.* **91** 157202
[5] Prellier W, Fouchet A and Mercey B 2003 *J. Phys.: Condens. Matter* **15** R1583
[6] Janisch R, Gopal P and Spaldin N A 2005 *J. Phys.: Condens. Matter* **17** R657
[7] Polyakov A Y *et al* 2004 *Mater. Sci. Semicond. Process.* **7** 77
[8] Coey J M D, Venkatesan M and Fitzgerald C B 2005 *Nat. Mater.* **4** 173
[9] Ahn G Y, Park S-I, Shim I-B and Kim C S 2004 *J. Magn. Magn. Mater.* **282** 166
[10] Ahn G Y, Park S-I, Kim S J, Lee B W and Kim C S 2005 *IEEE Trans. Magn.* **41** 2730
[11] Zhengwu J *et al* 2001 *Appl. Phys. Lett.* **78** 3824
[12] Potzger K *et al* 2006 *Appl. Phys. Lett.* **88** 052508
[13] Hong N H, Ruyter A, Prellier W and Sakai J 2004 *Appl. Phys. Lett.* **85** 6212
[14] Song C, Geng K W, Zeng F, Wang X B, Shen Y X, Pan F, Xie Y N, Liu T, Zhou H T and Fan Z 2006 *Phys. Rev.* B **73** 024405
[15] Ankudinov A L, Ravel B, Rehr J J and Conradson S D 1998 *Phys. Rev.* B **58** 7565
[16] Song C, Zeng F, Shen Y X, Geng K W, Xie Y N, Wu Z Y and Pan F 2006 *Phys. Rev.* B **73** 172412
[17] Prellier W, Fouchet A, Mercey B, Simon Ch and Raveau B 2003 *Appl. Phys. Lett.* **82** 3490
[18] Wang J Z, Peres M, Soares J, Gorochov O, Barradas N P, Alves E, Lewis J E, Fortunato E, Neves A and Monteiro T 2005 *J. Phys.: Condens. Matter* **17** 1719
[19] Roosendaal S J, Giebels I A M E, Vredenberg A M and Habraken F H P M 1998 *Surf. Interface Anal.* **26** 758
[20] Stenberg T, Vuoristo P, Keränen J, Mäntylä T, Büchler, Virtanen S, Schmuki P and Böhni H 1998 *Thin Solid Films* **312** 46
[21] Kolesnik S, Dabrowski B and Mais J 2003 *J. Appl. Phys.* **95** 2582
[22] Ando K, Saito H, Jin Z, Fukumara T, Kawasaki M, Matsumoto Y and Koinuma H 2001 *J. Appl. Phys.* **89** 7284
[23] Chen J J, Gao Y, Zeng F, Li D M and Pan F 2004 *Appl. Surf. Sci.* **223** 318
[24] Kaminski A and Das Sarma S 2002 *Phys. Rev. Lett.* **88** 247202
[25] Coey J M D, Venkatesan M, Stamenov P, Fitzgerald C B and Dorneles L S 2005 *Phys. Rev.* B **72** 024450
[26] Ogale S B *et al* 2003 *Phys. Rev. Lett.* **91** 077205
[27] Edmonds K W, Binns C, Baker S H, Thornton S C, Norris C, Goedkoop J B, Finazzi M and Brookes N B 1999 *Phys. Rev.* B **60** 472